

# Bayesian Inference with the $l_1$ -ball Prior: Solving Combinatorial Problems with Exact Zeros

Maoran Xu

Department of Statistics, University of Florida, Gainesville, USA

Leo L. Duan

Department of Statistics, University of Florida, Gainesville, USA

July 20, 2022

## Abstract

The  $l_1$ -regularization is very popular in the high dimensional statistics — it changes a combinatorial problem of choosing which subset of the parameter are zero, into a simple continuous optimization. Using a continuous prior concentrated near zero, the Bayesian counterparts are successful in quantifying the uncertainty in the variable selection problems; nevertheless, the lack of exact zeros makes it difficult for broader problems such as the change-point detection and rank selection. Inspired by the duality of the  $l_1$ -regularization as a constraint onto an  $l_1$ -ball, we propose a new prior by projecting a continuous distribution onto the  $l_1$ -ball. This creates a positive probability on the ball boundary, which contains both continuous elements and exact zeros. Unlike the spike-and-slab prior, this  $l_1$ -ball projection is continuous and differentiable almost surely, making the posterior estimation amenable to the Hamiltonian Monte Carlo algorithm. We examine the properties, such as the volume change due to the projection, the connection to the combinatorial prior, the minimax concentration rate in the linear problem. We demonstrate the usefulness of exact zeros that simplify the combinatorial problems, such as the change-point detection in time series, the dimension selection of mixture model and the low-rank-plus-sparse change detection in the medical images.

*Keywords::* Cardinality, Data Augmentation, Reversified Projection, Soft-Thresholding.

## 1 Introduction

The  $l_1$ -regularization has been a milestone in the high dimensional statistics. Since its introduction in the lasso regression for solving the variable selection problem [Tibshirani, 1996], it has inspired a rich class of algorithms and models — an incomplete list of representative works cover areas of regression [Efron et al., 2004, Zou and Hastie, 2005, Yuan and Lin, 2006], multivariate data analysis [Chen et al., 2001, Zou et al., 2006], graph estimation [Shojaie and Michailidis, 2010, Zhang and Zou, 2014, Fan et al., 2017], among others. For comprehensive reviews, see Meinshausen and Bühlmann [2006], and more recently Bühlmann and Van De Geer [2011].

One of the most appealing properties of  $l_1$ -regularization is that it induces exact zeros in the optimal solution, hence bypassing the need to decide which subset of the parameter should be zero. This is due to the well-know dual form of the  $l_1$ -norm penalty, as equivalent to constraining

the parameter on an  $l_1$ -ball centered at the origin. The “spikiness” of the  $l_1$ -ball in high dimension makes it possible for a sparse recovery of the signals [See Vershynin [2018] for a formal exposition].

In recent years, it has been demonstrated that the sparse property can be exploited beyond the simple tasks of variable selection. In particular, it can be used to build equivalence (or relaxation) to some complicated combinatorial problems, using the “ $l_1$ -trick” — we summarize it as an “*over-parameterize and sparsify*” strategy.

To give a few concrete examples, in the change-point detection of time series data, the fused lasso [Tibshirani et al., 2005] over-parameterizes each time point with an individual mean, then induces sparsity in the temporal increments/decrements; effectively, this leads to a step function that captures any abrupt temporal changes. For clustering problems, the sum-of-norms clustering [Lindsten et al., 2011, Tan and Witten, 2015] assigns a location parameter to every data point, then sparsifies the pairwise distance matrix; this induces only a few unique locations as the cluster centers. In the low-rank matrix smoothing/imputation, one uses an unconstrained matrix as the smoothed mean, then adding the nuclear norm regularization [Grave et al., 2011] as equivalent to sparsifying the singular values; this effectively achieves a rank selection on the matrix. These are just a few examples of the  $l_1$ -tricks; nevertheless, it is not hard to see the equivalent combinatorial problems would be quite difficult to handle directly.

Most of the above models have been developed with an optimization focus; in parallel, the Bayesian literature is expanding rapidly to address the uncertainty quantification problems, in particular: (i) how likely a parameter element is zero or non-zero? (ii) how much correlation there is between the non-zero elements? These questions are important for the downstream statistical inference, such as building credible intervals and testing hypotheses. Among the early work, the Bayesian lasso exponentiates the negative  $l_1$ -norm in a double exponential prior [Park and Casella, 2008]; however, it was discovered that except for the posterior mode, the posterior of the Bayesian lasso has very little concentration near zero, while the thin tails cause an underestimation of the non-zero signal. To address these issues, a rich class of continuous shrinkage priors have been proposed, with a large concentration in a neighborhood near zero and heavy tail to accommodate large signals. Examples include the horseshoe [Carvalho et al., 2010], generalized double Pareto [Armagan et al., 2013], Dirichlet-Laplace [Bhattacharya et al., 2015], Beta-prime [Bai and Ghosh, 2019], spike-and-slab lasso [Ročková and George, 2018]; among others. Due to the use of continuous priors, the posterior computation can be carried out efficiently using the Markov chain Monte Carlo methods [Bhattacharya et al., 2016]; this is advantageous compared to the classic spike-and-slab prior, which involves a combinatorial prior that selects a subset of parameter to be non-zero [Mitchell and Beauchamp, 1988].

In these Bayesian models, although the posterior are not exactly zero, the close-to-zero estimates are adequate for the common variable selection problems. However, for the above  $l_1$ -trick methods, it faces challenges to build the Bayesian equivalency using the continuous shrinkage priors. First, as we demonstrate in the change-point detection problem, the close-to-zero increments induced by the continuous shrinkage prior can accumulate over time, amounting to a non-trivial error. To better understand the issue, notice that the success of an  $l_1$ -trick would require some *transform* of the parameter to be zero (for example, the sum of changes over a long period of time in the change-point detection case). To that end, the continuous shrinkage prior placed on the individual elements, collectively, do not have a sufficiently large probability for the transform to be near zero. Second, there are problems in assigning a prior directly on the transform. Most importantly, the transform is often in a constrained space (for example, the distance matrix for points in  $\mathbb{R}^p$  being low-rank); hence the prescribed prior density is in fact incomplete, missing an intractable normalizing that could have an impact on the amount of shrinkage.

To address this issue, as well as to encourage developing novel combinatorial models, we

propose a new strategy: starting from a continuous random variable with unconstrained support, we project it onto the  $l_1$ -ball. This induces a distribution allowing the random variable to contain exact zeros. Since the projection is a continuous and differentiable transformation almost surely, we can use the popular off-the-shelf sampling algorithms such as the Hamiltonian Monte Carlo for the posterior computation. We are certainly not the first to consider a projection / transformation-approach for Bayesian modeling. For example, Gunn and Dunson [2005] used it for handling monotone and unimodal constraints, Lin and Dunson [2014] for inducing monotone Gaussian process, Jauch et al. [2020] for satisfying orthonormal matrix constraint, and most recently, Sen et al. [2018] for a theoretic study on the projection of the posterior. Although we are inspired by those methods, our focus is not to satisfy the parameter constraints, but use the *boundary* of a constrained set to induce a low-dimensional measure — in this case, any point outside the  $l_1$ -ball will be projected onto the boundary, we obtain a positive probability for the random variable (or its transform) to contain both continuous elements and exact zeros. To our best knowledge, this idea is new.

We will illustrate the details of the projection, its properties such as the volume change due to the projection, the connection to the combinatorial prior, the minimax concentration rate in the linear problem. In the applications, we will demonstrate the usefulness of  $l_1$ -tricks in a few Bayesian models of combinatorial problems, such as the dimension selection in the finite mixture model and the low-rank matrix smoothing with an application in the medical image analysis.

## 2 The $l_1$ -ball Prior

In this section, we address three important questions: (i) how does the  $l_1$ -ball projection change a continuous random variable, into a mixed-type random variable containing both continuous elements and zeros? (ii) how to calculate the associated probability after the projection? (iii) how to determine the radius of the  $l_1$ -ball?

### 2.1 Inducing Sparsity on the $l_1$ -ball

Starting with a parameter space  $\mathbb{R}^p$ , we consider the  $l_1$ -ball with a given radius  $r > 0$  and closed boundary,

$$\mathbb{B}_r = \{x \in [-r, r]^p : \|x\|_1 \leq r\}.$$

We denote the interior set by  $\mathbf{int} \mathbb{B}_r = \{x \in (-r, r)^p : \|x\|_1 < r\}$ , and boundary set by  $\mathbf{bd} \mathbb{B}_r = \{x : \|x\|_1 = r\}$ . For any point  $\beta \in \mathbb{R}^p$ , we can project it onto the  $l_1$ -ball, by solving the following optimization problem,

$$\theta = P_{\mathbb{B}_r}(\beta) = \arg \min_{\|x\|_1 \leq r} \|\beta - x\|_2^2.$$

This problem is strictly convex — that is, for every  $\beta$ , there is only one optimal solution  $\theta = P_{\mathbb{B}_r}(\beta)$  (i.e., the mapping is measurable). Here we present a simple solution [modifying from Duchi et al. [2008]]: if  $\|\beta\|_1 \leq r$ , let  $\theta = \beta$ ; If  $\|\beta\|_1 > r$ ,

$$\begin{aligned} & \text{sort } \beta \text{ so that } |\beta_{(1)}| \geq \dots \geq |\beta_{(p)}|, \\ c &:= \max\{j : |\beta_{(j)}| > \frac{\mu_j}{j}, \mu_j = (\sum_{i=1}^j |\beta_{(i)}| - r)_+\}, \\ \theta_i &:= \text{sign}(\beta_i) \max(|\beta_i| - \frac{\mu_c}{c}, 0), \end{aligned} \tag{1}$$

where  $(x)_+ = \max\{x, 0\}$ .

We now examine how this projection changes a simple continuous random variable. Suppose  $\beta \in \mathbb{R}^p$  is a continuous random variable, in a probability space  $(\mathbb{R}^p, \mathcal{B}(\mathbb{R}^p), \nu)$ , with  $\nu$  its measure absolutely continuous with respect to the Lebesgue measure in  $\mathbb{R}^p$ , and  $\pi_\beta$  the associated density. We can compute the probability for  $\theta$  in any set  $\mathcal{A}$  in  $\mathbb{B}_r$ :

$$\text{pr}(\theta \in \mathcal{A}) = \int_{\mathbb{R}^p} \mathbb{I}[P_{\mathbb{B}_r}(x) \in \mathcal{A}] \pi_\beta(x) dx, \quad (2)$$

where  $\mathbb{I}(E) = 1$  if the event  $E$  is true, otherwise takes value 0. Combining (1) and (2), we see two interesting results when projecting  $\beta : \|\beta\|_1 > r$ :

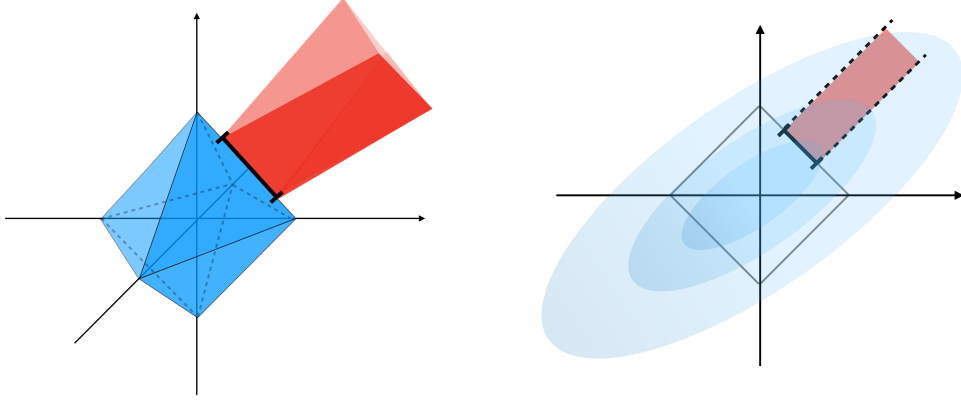
1. It yields  $\theta$  with  $\|\theta\|_1 = r$ , hence in the boundary. Since all the points outside the ball will be projected to  $\theta \in \text{bd } \mathbb{B}_r$ , the boundary set has a positive probability.
2. If the projection has  $c < p$ , there will be  $(p - c)$  elements with  $\theta_i = 0$ .

In addition, in the computation section, we will show that:

3. The projection  $P_{\mathbb{B}_r}$  is a continuous and differentiable function of  $\beta$  almost surely with respect to  $\nu$ , which allows the use of the Hamiltonian Monte Carlo for estimation.

These results suggest a simple way to develop an exactly sparse prior: assigning a continuous prior  $\pi_\beta$  on  $\beta$  and set  $\theta = P_{\mathbb{B}_r}(\beta)$ . We denote the induced prior by  $\pi_\theta(\theta)$ .

To illustrate the geometric intuition, we show the projection in  $\mathbb{R}^3$  (Figure 1) — projecting  $\beta$  from a multivariate Gaussian to  $\theta \in \mathbb{B}_r$  gives us positive probability  $\text{pr}[\theta = (x_1, 0, x_3)] > 0$ , which equals to the Gaussian measure in the wedge region outside  $\mathbb{B}_r$ . Note that this is quite different from the conventional setting where  $\theta$  is assigned a continuous prior in  $\mathbb{R}^p$ , for which fixing any  $\theta_i = 0$  would cause the probability to collapse to zero.



(a) All the points  $\beta$  in the red area are projected to  $\theta$  in the line segment  $\{(x, 0, r - x) : 0.2 < x < 0.8\}$ , which contains exact zero  $\theta_2 = 0$ .

(b) Sectional view in 2-dimensions: the probability of  $\theta$  in the line segment is equal to the measure of  $\beta$  over the area in the red, which is positive.

Figure 1: Projecting a continuous Gaussian  $\beta \in \mathbb{R}^3$  to  $\theta$  onto an  $l_1$ -ball  $\mathbb{B}_r$  (the right panel shows a density contour in 2-dimensions): the boundary set of  $\theta$  containing exactly zero has a positive probability. For example, the probability of  $\theta$  in the line segment  $\{(x, 0, r - x) : 0.2 < x < 0.8\}$  is equal to the probability of  $\beta$  over the red region.



## 2.2 Deriving a Closed-form Kernel via the Data Augmentation

Using the above intuition, we can now formally derive the prior of  $\theta$ . This can be obtained in a simple closed-form with data augmentation. When  $\theta \in \mathbf{bd} \mathbb{B}_r$ , the elements of  $\theta$  contain both zeros and continuous random variables. Therefore, we associate  $\theta$  with a prior *kernel*  $\pi_\theta(\theta)$ , a function  $\pi_\theta : \mathbb{B}_r \rightarrow [0, \infty)$ , as the mix of probability mass and density functions, integrable to 1 over  $\mathbb{B}_r$  (we slightly abuse the notation to use  $\pi_\cdot$  to denote both the kernel and distribution).

To introduce some notations, we let  $[p] = \{1, \dots, p\}$  be the full element indices, and  $C = \{i \in [p] : \theta_i \neq 0\}$  a subset for those non-zero elements with  $c := |C|$ . And we use subscript to denote the non-zero sub-vector  $\theta_C = (\theta_i)_{i \in C}$ .

We now divide the  $l_1$ -ball projection into two steps: (i) one-to-one transform of  $\beta$  into a set of latent variables; (ii) integrating over those falling below zero, as equivalent to the zero-thresholding in (1).

The step (i) produces the following latent variables:

$$t_i := |\beta_i| - \frac{\mu}{c}, \quad s_i := \text{sign}(\beta_i) \quad \text{for } i \in [p],$$

$$\mu := \mu_c, \quad c = \max\{j : |\beta_{(j)}| > \frac{\mu_j}{j}, \mu_j = (\sum_{i=1}^j |\beta_{(i)}| - r)_+\}.$$

We denote this transformation by  $f(\beta) = (t, s, \mu)$ , which will be shown in the theory section is one-to-one, hence we can denote the inverse function as  $f^{-1}$  and use the change-of-variable method to compute the probability kernel for  $\pi_{t,s,\mu}(t, s, \mu)$ .

**Theorem 1** (volume preserving transformation). *With  $(t, s, \mu) = f(\beta)$  defined as the above, for any proper density  $\pi_\beta$ , the absolute determinant of the Jacobian, denoted by  $|J_f|$ , is one. Therefore,*

$$\pi_\beta(\beta) = \pi_{t,s,\mu}[f(\beta)].$$

**Remark 1.** *The constant  $|J_f| = 1$  shows that  $f$  is a volume-preserving transform, hence the derived kernel is invariant to the number of non-zeros  $c$ . This is especially useful for the posterior computation, since the posterior kernel is continuous even when the number of zeros changes from  $c$  to  $c'$ .*

The step (ii) produces a sparse  $\theta$  via the signed zero-thresholding  $\theta_i = s_i(t_i)_+$ . Equivalently, we can view  $\pi_\theta(\theta)$  as the marginal form for  $\pi_{t,s,\mu}(t, s, \mu)$ , summed over those  $(s_i, t_i) : t_i < 0$  and  $\mu > 0$ :

$$\begin{aligned} \pi_\theta(\theta) &= \pi_\theta(\theta_i = s_i t_i \text{ for } i \in C; \theta_i = 0 \text{ for } i \notin C) \\ &= \sum_{s_i = \pm 1 \text{ for } i \notin C} \int_0^\infty \int_{(-\mu/c, 0)^{p-c}} \pi_{t,s,\mu}(t, s, \mu) dt_{[p] \setminus C} d\mu. \end{aligned}$$

To show the details of the above results, we use a working example: consider an independent double exponential  $\beta_i \sim \text{DE}(0, \lambda_i)$ ,  $\pi(\beta_i) = 1/(2\lambda_i) \exp(-|\beta_i|/\lambda_i)$ , with  $\lambda_i > 0$ . Transforming  $\beta$  to  $(t, s, \mu)$ , we obtain the prior kernel:

$$\pi_{t,s,\mu}(t, s, \mu) = \prod_{i=1}^p \frac{1}{2\lambda_i} \exp(-\frac{\mu/c}{\lambda_i}) \exp(-\frac{t_i}{\lambda_i}), \quad (3)$$

subject to constraints  $t_i > -\mu/c$  and  $\sum_{i=1}^p (t_i)_+ = r$ . In this special case, we do have a closed-form marginal probability:

$$\begin{aligned} \text{pr}(\theta_i = 0) &= 1 - \exp(-\frac{\mu/c}{\lambda_i}), \quad \text{pr}(|\theta_i| > 0) = \exp(-\frac{\mu/c}{\lambda_i}), \\ \pi_\theta(\theta \mid |\theta_i| > 0) &= \frac{1}{2\lambda_i} \exp(-\frac{|\theta_i|}{\lambda_i}). \end{aligned} \tag{4}$$

**Remark 2.** *To clarify, in this article, we choose to present the double exponential  $\pi_\beta$  for the ease of integration, which is useful for a tractable theoretic analysis later. In practice, we can choose any continuous  $\pi_\beta$ , such as the multivariate Gaussian. The volume preserving property and convenient computation will hold in general.*

In general, the above marginalization may not be tractable, however, we can use the data augmentation [Tanner and Wong, 1987] for the posterior estimation. To elaborate, let  $\mathcal{L}(y; \theta, \eta)$  be the likelihood,  $y$  the data,  $\eta$  some other parameter with prior  $\pi_\eta(\eta \mid \beta)$  [or  $\pi_\eta(\eta)$  independent from  $\beta$ ], we can sample the posterior of  $(t, s, \mu)$  and  $\eta$  via:

$$\pi(t, s, \mu, \eta \mid y) \propto \pi_\eta[\eta \mid f^{-1}(t, s, \mu)] \pi_{t,s,\mu}(t, s, \mu) \mathcal{L}[y; \theta, \eta : \theta_i = s_i(t_i)_+ \text{ for } i \in [p]].$$

Equivalently, changing the variable  $(t, s, \mu)$  into  $\beta$ , we have a very simple posterior of  $\beta$ :

$$\pi(\beta, \eta \mid y) \propto \pi_\eta(\eta \mid \beta) \pi_\beta(\beta) \mathcal{L}[y; P_{\mathbb{B}_r}(\beta), \eta]. \tag{5}$$

This means, we can first obtain the posterior samples of  $\eta$  and  $\beta$ , compute  $\theta = P_{\mathbb{B}_r}(\beta)$  for each sample of  $\beta$ , then discard the intermediate information in  $(t, s, \mu)$ .

### 2.3 Prior on the Radius via a Random Threshold

Thus far, we have treated  $r = \|\theta\|_1$  (the radius of  $\mathbb{B}_r$ ) as given. As we do not know  $r$  as a priori, we will treat it as an unknown parameter, assign a prior and estimate it from the posterior.

There are more than one ways to choose the prior on  $r$ . For example, one could consider a dimension-adaptive prior on  $r$ , as we will use in the theory section. On the other hand, one may be interested in imposing a prior belief on the percentage of zeros in  $\theta$ ; hence we present a strategy here.

Note that the projection involves a soft-thresholding  $\theta_i = \text{sign}(\beta_i)(|\beta_i| - \mu/c)_+$  with a threshold  $\tilde{\mu} = \mu/c$ . If we are given  $\tilde{\mu} = \mu/c$  and  $\beta$  as in (1), then  $r$  is completely determined as:

$$r = \sum_{i=1}^p (|\beta_i| - \tilde{\mu})_+.$$

Therefore, a prior choice on  $\pi_{\tilde{\mu}}(\tilde{\mu})$  is a choice on  $\pi_r(r)$ . As shown in Figure 2,  $\tilde{\mu}$  divides the distribution  $\pi(|\beta|)$  into two parts, corresponding to  $|\beta_i| \leq \tilde{\mu}$  associated with the point mass  $\theta_i = 0$ , and  $|\beta_i| > \tilde{\mu}$  associated with  $|\theta_i| > 0$ .

Therefore, we can choose  $\tilde{\mu}$  based on a random quantile of  $(|\beta_1|, \dots, |\beta_p|)$ :

$$\begin{aligned} w &\sim \text{Beta}(a_w, b_w), \\ \tilde{\mu} &= (1 - w)\text{-quantile of } (|\beta_1|, \dots, |\beta_p|), \end{aligned}$$

where  $(a_w, b_w)$  are hyper-parameters imposing the prior belief on  $w$ . Given  $w$ , there will be  $(pw)$  elements of  $\theta_i$ 's equal to zero.

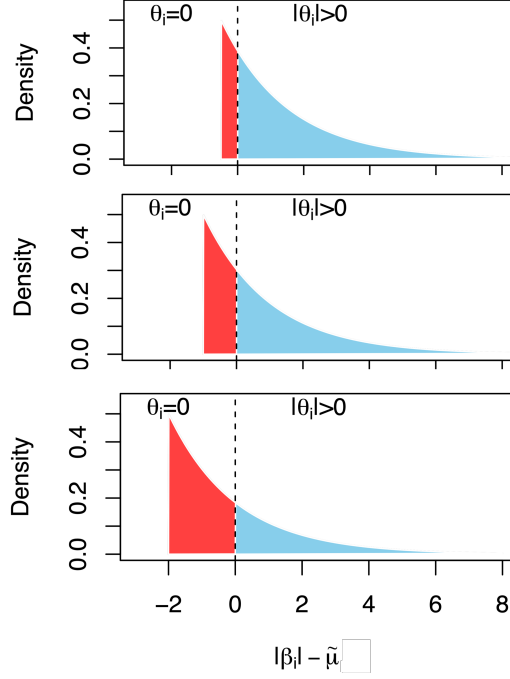


Figure 2: A soft-thresholding view of the  $l_1$ -ball prior, when the radius  $r$  is treated as a free parameter — this is equivalent to having a free threshold parameter  $\tilde{\mu}$ , which divides the distribution  $\pi(|\beta|)$  into two parts, corresponding to  $|\beta_i| \leq \tilde{\mu}$  and  $\theta_i = 0$  (red), or  $|\beta_i| > \tilde{\mu}$  and  $|\theta_i| > 0$  (blue).

### 3 Theoretical Study

We now focus on a more theoretical study on the  $l_1$ -ball prior.

First, we show that the augmented transform  $f$  in the  $l_1$ -projection is indeed invertible. Recall that  $f : \mathbb{R}^p \rightarrow \{(t, s, \mu) \in \mathbb{R}^p \times \{1, -1\}^p \times \mathbb{R}_+ : \sum_{i=1}^p (t_i)_+ = r, t_i \geq -\mu/|C|\}$ .

**Theorem 2.** Consider another transform  $\beta = g(t, s, \mu)$  with  $C = \{i : t_i > 0\}$ , and let

$$\beta_i = s_i(t_i + \frac{\mu}{|C|}), \quad (6)$$

where its domain satisfies the following:  $s_i \in \{-1, 1\}$ ; if  $\sum_{i \in C} t_i = r$ , then for  $i \notin C$ ,  $-\mu/|C| \leq t_i \leq 0$  and  $\mu \geq 0$ ; if all  $t_i \geq 0$  and  $\sum t_i < r$ , then  $\mu = 0$ . If  $|C| = 0$ , all  $\beta_i = 0$ . Then  $g$  is the inverse mapping of  $f$ , that is:

$$f[g(t, s, \mu)] = (t, s, \mu), \quad g[f(\beta)] = \beta.$$

**Remark 3.** Broadly speaking, this gives an “projection-based data augmentation” scheme for any sparse  $\theta$  (such as the one in the spike-and-slab prior): we can augment  $(t_i, s_i)$ ’s for those  $\theta_i = 0$  and a  $\mu \geq 0$ , and then apply  $\beta = g(t, s, \mu)$ . The produced  $\beta$  is a continuous embedding for  $\theta$ .

Next, we establish a link between some special form of the  $l_1$ -ball prior to the combinatorial prior that chooses a subset of  $\theta$  to be zero [Castillo et al., 2015]. When  $\beta_i \stackrel{\text{iid}}{\sim} \text{DE}(0, \lambda)$ , we can further integrate and obtain two simple marginal forms.

**Theorem 3.** *If  $\pi_\beta(\beta) = \prod_i (2\lambda)^{-1} \exp(-|\beta_i|/\lambda)$  with  $\lambda > 0$ , then for  $\theta \in \text{int}\mathbb{B}_r$ ,  $\pi_\theta(\theta \mid r, \lambda) = \prod_i (2\lambda)^{-1} \exp(-|\theta_i|/\lambda) \mathbb{I}(\|\theta\|_1 < r)$ , and for  $\theta \in \text{bd}\mathbb{B}_r$ ,*

$$\pi_\theta(\theta \mid r, \lambda) = \frac{(2\lambda)^{-|C|}}{\binom{p}{|C|}} \lambda \exp\left(-\frac{r}{\lambda}\right) \mathbb{I}(\|\theta\|_1 = r), \quad (7)$$

where  $C = \{i \in [p] : \theta_i \neq 0\}$ .

Further marginalizing over  $\theta$  on  $\{\theta : \|\theta\|_1 = r, \sum_{i=1}^p \mathbb{I}(\theta_i \neq 0) = j\}$ , we can obtain a discrete prior distribution on  $|C|$ .

**Corollary 1.** *If  $\pi_\beta(\beta) = \prod_i (2\lambda)^{-1} \exp(-|\beta_i|/\lambda)$  with  $\lambda > 0$ , then the marginal prior  $\pi(|C|; r)$  follows a truncated Poisson distribution, with*

$$\text{pr}(|C| = j \mid r) = \frac{(r/\lambda)^{j-1}}{(j-1)!} \exp\left(-\frac{r}{\lambda}\right), \quad (8)$$

for  $j = 1, \dots, (p-1)$ ; and  $\text{pr}(|C| = p \mid r) = 1 - \sum_{j=1}^{p-1} (r/\lambda)^{j-1}/(j-1)! \exp(-r/\lambda)$ .

In the above, we can see how the radius impacts the the level of sparsity:

$$\begin{aligned} \mathbb{E}(|C| - 1) &= \sum_{j=1}^{p-1} (j-1) \frac{(r/\lambda)^{j-1}}{(j-1)!} \exp\left(-\frac{r}{\lambda}\right) + (p-1) \sum_{j=p}^{\infty} \frac{(r/\lambda)^{j-1}}{(j-1)!} \exp\left(-\frac{r}{\lambda}\right) \\ &\leq r/\lambda, \end{aligned}$$

where the inequality is due to  $(p-1) \leq (j-1)$  for  $j \geq p$  and the expectation of an untruncated Poisson( $r/\lambda$ ) is  $r/\lambda$ . Therefore, a smaller  $r$  favors a smaller  $|C|$  and more  $\theta_i$ 's to be zero.

Lastly, we study the posterior convergence rate using the above prior. Since the rate is highly dependent on the form of the likelihood, we choose to narrow our focus on the well-studied linear regression model, and demonstrate an equivalently optimal rate as the existing approaches. For a comprehensive review on this topic, see Castillo and van der Vaart [2012].

We follow the standard theoretic analysis and assume  $y_i$  and  $\theta_i$  are re-scaled by  $1/\sigma$ , so that  $y_i \sim \text{N}(x_i^T \theta, 1)$ , while assuming there is an oracle  $\theta^0 \in \mathbb{R}^p$ , with the true cardinality  $c_0 \neq 0$ . In practice, since we do not know  $\sigma^2$  we can assign a prior on  $\sigma^2 \sim \text{Inverse-Gamma}(\gamma_{\sigma^2,1}, \gamma_{\sigma^2,2})$ , and additionally let  $\theta$  scale with  $\sigma$ . To provide a more straightforward result, we choose a simple prior on  $r$ ,  $\pi_r(r) = \alpha^{-1} \exp(-r/\alpha)$  with  $\alpha$  a parameter to determine. Multiplying it to (8) and integrating over  $r$ , and we obtain the marginal model selection probability under the  $\pi_r(r)$ :

$$\text{pr}(|C| = j; \lambda, \alpha) = \frac{\lambda/\alpha}{(1 + \lambda/\alpha)^j}, \quad (9)$$

for  $j = 1, \dots, (p-1)$ ; and  $\text{pr}(|C| = p; \lambda, \alpha) = 1 - \sum_{j=1}^{p-1} \lambda/\alpha (1 + \lambda/\alpha)^{-j} = (1 + \lambda/\alpha)^{-(p-1)}$ . And

$$\pi_\theta(\theta; \lambda, \alpha) = \frac{(2\lambda)^{-|C|}}{\binom{p}{|C|}} \lambda/\alpha \exp\left[-(1/\lambda + 1/\alpha)^{-1} \|\theta\|_1\right], \quad (10)$$

for  $|C| = 1, \dots, (p-1)$ . We now present the convergence result.

**Theorem 4.** *If the data are generated from  $y_i = X_{i,\cdot}^T \theta^0 + \epsilon_i$ ,  $\epsilon_i \stackrel{iid}{\sim} N(0, 1)$ , with  $(\lambda, \alpha)$  chosen as  $\lambda = b_1 p^{b_2} / \|X\|_{2,\infty}$ ,  $\alpha = p^{b_3} / \|X\|_{2,\infty}$ ,  $b_1 > 0$ ,  $b_2 > b_3$ ,  $b_3 \leq 1$ , and  $\|X\|_{2,\infty} := \max_j \sqrt{\sum_i X_{i,j}^2}$ , with sufficiently large  $M$ , then as  $n, p \rightarrow \infty$ :*

- (Cardinality) *For estimating the true cardinality  $c_0$ ,*

$$\sup_{\theta^0} \mathbb{E}_{\theta^0} \Pi \left( \theta : |C_\theta| > c_0 \left[ 1 + \frac{M}{b_2 - b_3} \left( 1 + \frac{16}{\phi(C_0)^2} \frac{\lambda^*}{2\|X\|_{2,\infty} \sqrt{\log p}} \right) \right] \middle| Y \right) \rightarrow 0,$$

where  $\lambda^* = \|X\|_{2,\infty} (b_1 p^{b_2} + p^{b_3}) / (b_1 p^{b_2} p^{b_3})$ .

- ( $l_2$ -recovery) *The recovery of true  $\theta^0$  has*

$$\sup_{\theta^0} \mathbb{E}_{\theta^0} \Pi \left( \theta : \|\theta - \theta^0\|_2 > \frac{M}{\psi(C_0)^2} \frac{\sqrt{c_0 \log p}}{\|X\|_{2,\infty} \phi(C_0)} \middle| Y \right) \rightarrow 0,$$

- ( $l_\infty$ -recovery) *For every  $\eta > 0$ , any  $d_0 < \eta^2 [1 + 2/(b_2 - b_3)]^{-1} / 8$ , and  $c_n$  such that  $c_n (b_1 p^{b_2} + p^{b_3}) \sqrt{\log p} / (b_1 p^{b_2} p^{b_3}) \rightarrow 0$ , for the set  $\mathcal{C}^* = \{C_0 : \phi(C_0) \geq \eta, \psi(C_0) \geq \eta, c_0 \leq c_n, c_0 \leq d_0 mc(X)^{-1}\}$ , then the recovery of true  $\theta^0$  has*

$$\sup_{\theta^0 : C_0 \in \mathcal{C}^*} \mathbb{E}_{\theta^0} \Pi \left( \theta : \|\theta - \theta^0\|_\infty > M \frac{\sqrt{\log p}}{\|X\|_{2,\infty}} \middle| Y \right) \rightarrow 0.$$

In the above,  $mc(X) = \max_{i \neq j} \frac{|X_{\cdot,i}^T X_{\cdot,j}|}{\|X_{\cdot,i}\|_2 \|X_{\cdot,j}\|_2}$  is the mutual coherence, and  $\phi(C), \psi(C)$  are the compatibility numbers for matrix  $X$  that we give the definitions in the appendix.

In the appendix, we provide the results showing the convergence rate using simulations.

## 4 Extension: Generalized $l_1$ -ball Prior

We now demonstrate that the  $l_1$ -ball projection can be generalized to create prior such that some transform of  $\theta$  is sparse. Specifically, let  $h : \mathbb{R}^p \rightarrow \mathbb{R}^d$ , we use the following projection:

$$\theta = P_{\mathbb{B}_{h,r}}(\beta) = \underset{z : \|h(z)\|_1 \leq r}{\operatorname{argmin}} \|z - \beta\|_2^2. \quad (11)$$

For the regularity, we restrict the focus to when  $\|h(z)\|_1$  is convex — when it is satisfied, the level set  $\{z : \|h(z)\|_1 \leq r\}$  is a convex set, making the Euclidean projection unique hence a measurable mapping. This includes a large class of useful functions for the  $l_1$ -tricks, such as  $h(z) = Dz$  with  $D \in \mathbb{R}^{d \times p}$  as in the fused lasso, change-point detection, linear trend filter; and  $\|h(z)\|_1 = \sum_k \sqrt{\sum_j z_{k(j)}^2}$  as in the grouped lasso. We refer to  $\{z : \|h(z)\|_1 \leq r\}$  as a generalized  $l_1$ -ball, denoted by  $\mathbb{B}_{h,r}$ . Clearly, the  $l_1$ -ball is a special case with  $h(z) = z$ .

The above projection may not have a closed-form solution, however, it can be equivalently written via the splitting technique:

$$\theta = \underset{z : h(z) = w, \|w\|_1 \leq r}{\operatorname{argmin}} \|z - \beta\|_2^2 + \eta^T [h(z) - w] + \frac{1}{2\rho} \|h(z) - w\|_2^2,$$

where  $\rho > 0$  and  $\eta \in \mathbb{R}^d$  is Lagrangian multiplier (the values of  $\rho$  and  $\eta$  do not impact the convergence). Using  $\kappa = \rho\eta$ , the optimal solution can be computed using the alternating direction method of multipliers (ADMM) algorithm [Boyd et al., 2011], that iterates in:

$$\begin{aligned} z &\leftarrow \underset{z \in \mathbb{R}^p}{\operatorname{argmin}} [\|z - \beta\|_2^2 + \frac{1}{2\rho} \|h(z) - w + \kappa\|_2^2], \\ w &\leftarrow P_{\mathbb{B}_r}[h(z) + \kappa], \\ \kappa &\leftarrow \kappa + h(z) - w, \end{aligned} \tag{12}$$

until it converges, and then set  $\theta$  to be equal to  $z$ . Note that this algorithm contains a simple projection to the  $l_1$ -ball, as in (1).

Again, starting from a continuous  $\beta \sim \pi_\beta$  in  $\mathbb{R}^p$ , the projection  $\theta = P_{\mathbb{B}_{h,r}}(\beta)$  gives a new prior distribution, that we refer to as the generalized  $l_1$ -ball prior.

**Remark 4.** *It is important to point out that, even though  $P_{\mathbb{B}_{h,r}}(\beta)$  may not have a closed-form,  $P_{\mathbb{B}_{h,r}}(\beta)$  is still a continuous function of  $\beta$ , and differentiable almost surely with respect to the distribution of  $\beta$ . We will explain in the next section.*

To give a concrete example, we consider the sparsity imposed in the fused lasso,  $h(z) = Dz$  with  $D$  a  $(2p-1) \times p$  matrix corresponding to  $\|Dz\|_1 = \sum_{i=1}^p |z_i| + \sum_{i=2}^p |z_i - z_{i-1}|$ . It is not hard to see that, in this case, the first line of (12) can be solved in closed-form  $z \leftarrow [(2\rho)^{-1}D^T D + I]^{-1} \{\beta + (2\rho)^{-1}D^T(w - \kappa)\}$ ; hence we can rapidly obtain the projection.

Further, since  $D$  has rank  $p$ ,  $\{w \in \mathbb{R}^{2p-1} : w = D\theta\}$  is in a low-dimensional space, with the dimensionality at most  $p$ . This generalized  $l_1$ -ball projection creates a sparse prior for  $D\theta$  in a space that would be otherwise difficult to define directly.

## 5 Continuous Hamiltonian Monte Carlo for Posterior Computation

The Hamiltonian Monte Carlo is a powerful method for sampling the posterior distribution. It uses the Hamiltonian dynamics to propose a new state of parameter and accept it using the Metropolis-Hastings criterion. Due to the energy-preserving property, the Hamiltonian dynamics is capable of producing proposal that is far away from the current state, while often enjoying high acceptance rate. Neal [2011] provides an introduction on this algorithm.

One limitation, however, is that the common algorithm in the Hamiltonian Monte Carlo (such as the one implemented in Stan) only works on the continuous random variable under a continuous posterior density. Although some data augmentation methods are proposed for the binary discrete random variable, such as Pakman and Paninski [2013], they create discontinuity in the augmented posterior. To briefly explain, when a binary variable changes from 0 to 1, the likelihood will have a sudden jump that breaks the energy-preserving property of Hamiltonian dynamics. To handle this issue, one needs a modified algorithm known as the discontinuous Hamiltonian Monte Carlo [Nishimura et al., 2020].

Interestingly, the  $l_1$ -ball priors (including the generalized  $l_1$ -ball priors) are free from this issue, as long as  $\pi_\beta$  is continuous in  $\beta$  and the likelihood is continuous in  $\theta$ . Intuitively, for the  $l_1$ -ball prior, as  $\beta_i$  reduces in magnitude,  $\theta_i$  gradually changes toward 0 and stays at 0 after passing below the threshold — therefore, the projection function is continuous. We now formalize this intuition using the property of the proximal mapping, then briefly explain the Hamiltonian Monte Carlo algorithm.

## 5.1 Almost Sure Smoothness of the Posterior

We first introduce the concept of the proximal mapping, defined as

$$\text{prox}_g(x) = \underset{z}{\operatorname{argmin}} \{g(z) + \|x - z\|_2^2/2\},$$

with  $g$  a lower-semicontinuous and convex function. This mapping is routinely used in the optimization literature [Beck, 2017]. Now we choose  $g = \mathcal{X}_{\mathbb{B}_{h,r}}$ , the characteristic function of a set (a generalized  $l_1$ -ball), which takes value 0 in  $\mathbb{B}_{h,r}$  and takes  $\infty$  otherwise. Since  $\mathbb{B}_{h,r}$  is a convex set, this means that the projection  $P_{\mathbb{B}_{h,r}}(\beta)$  is a proximal mapping.

As a useful property, the proximal mapping is Lipschitz continuous with the Lipschitz constant 1 (Beck [2017], Theorem 6.42); in our case,

$$\|P_{\mathbb{B}_{h,r}}(\beta_1) - P_{\mathbb{B}_{h,r}}(\beta_2)\|_2 \leq \|\beta_1 - \beta_2\|_2.$$

Further, by the Rademacher's Theorem (Federer [2014], Thm. 3.1.6), any Lipschitz continuous function is differentiable almost everywhere with respect to the measure on its input — in our case, the chosen  $\pi_\beta$  before the projection.

As the result, when the likelihood function is continuous in  $\theta$ , it is continuous in  $\beta$  using variable transformation  $\theta = P_{\mathbb{B}_{h,r}}(\beta)$ , hence the posterior is a continuous function of  $\beta$  as well. Further, if the likelihood is smooth with respect to  $\theta$  almost surely, then the posterior is smooth almost surely as well. This means, we can simply run the continuous Hamiltonian Monte Carlo.

## 5.2 Brief Review of the Algorithm

For the sake of completeness, we now briefly review the Hamiltonian Monte Carlo algorithm.

To sample the parameter  $q = (\beta, \eta)$  from target distribution  $q \sim \pi_{q|y}(\cdot)$ , the Hamiltonian Monte Carlo considers an auxiliary momentum variable  $v$  with density  $\pi_v(v)$ , and samples from the joint distribution  $\pi(q, v) = \pi_{q|y}(q)\pi_v(v)$ . The potential energy and kinetic energy are defined to be  $U(q) = -\log \pi_{q|y}(q)$  and  $K(v) = -\log \pi_v(v)$ , and the total Hamiltonian energy function is denoted by  $H(q, v) = U(q) + K(v)$ . Our choice of  $\pi_v(v)$  is the multivariate Gaussian density  $N(0, I)$ , with the kinetic energy  $K(v) = v^T v/2$ .

At each state  $(q, v)$ , a new proposal is generated by simulating Hamiltonian dynamics, which satisfy the Hamilton's equations:

$$\frac{\partial q}{\partial t} = \frac{\partial H(q, v)}{\partial v} = v, \quad \frac{\partial v}{\partial t} = -\frac{\partial H(q, v)}{\partial q} = -\frac{\partial \log \pi_{q|y}(q)}{\partial q}. \quad (13)$$

The exact solution for (13) is often intractable, but we can numerically approximate the solution to the differential equations by algorithms such as the leapfrog scheme. The leapfrog is a reversible and volume-preserving integrator, which updates the evolution  $(q^{(t)}, v^{(t)}) \rightarrow (q^{(t+\epsilon)}, v^{(t+\epsilon)})$  via

$$v \leftarrow v + \frac{\epsilon}{2} \frac{\partial \log \pi_{q|y}(q)}{\partial q}, \quad q \leftarrow q + \epsilon v, \quad v \leftarrow v + \frac{\epsilon}{2} \frac{\partial \log \pi_{q|y}(q)}{\partial q}. \quad (14)$$

The proposal  $(q^*, v^*)$  is generated by taking  $L$  leapfrog steps from current state  $(q^{(0)}, v^{(0)})$ , then accepted using the Metropolis-Hastings algorithm, with the acceptance probability:

$$\min\{1, \exp[-H(q^*, v^*) + H(q^{(0)}, v^{(0)})]\}.$$

For the step size  $\epsilon$  and the leapfrog steps  $L$ , we use the No-U-Turn Sampler [Hoffman and Gelman, 2014] to automatically adapt these working parameters. In the case of  $P_{\mathbb{B}_{h,r}}(\beta)$  not having a closed-form, we use the numerical method to evaluate  $\partial P_{\mathbb{B}_{h,r}}(\beta)/\partial \beta$ .

### 5.3 Point Estimate and Credible Region for the Low Dimensional Parameter

Uncertainty quantification often relies on the calculation of the credible region: for a certain function of the random variable  $g(\theta)$  (such as  $\theta$  itself, fitted value  $X\theta$ , etc.), we want a region  $R_g$ , such that

$$\text{pr}[g(\theta) \in R_g \mid y] = 1 - \alpha,$$

with some given  $\alpha \in (0, 1)$ .

A common way to approximate  $R_g$  is to take the posterior samples of  $g(\theta)$ , and take point-wise quantiles in the elements of the  $g(\theta)$  output, while adjusting for multiplicity. However, this is sub-optimal for a sparse  $\theta$  and/or an intrinsically low-dimensional  $g(\theta)$  (such as the piece-wise linear  $X\theta$ ), for two reasons: (i) the multiplicity adjustment is often too conservative, making the credible region too large (that is, the associated probability is in fact much larger than  $1 - \alpha$ ); (ii) the combination of the point-wise credible intervals is often no longer low-dimensional.

To bypass these issues, we use the solution from Breth et al. [1978] based on the *top*  $(1 - \alpha)$  *posterior density region*:

$$R_g = \{g(\theta) : \Pi_\theta(\theta \mid y) \geq \kappa_\alpha\},$$

where  $\kappa_\alpha$  is a threshold that makes the region having a probability  $1 - \alpha$ . In practice, we can approximate  $\kappa_\alpha$  by simply calculating the posterior kernels for all the samples, then take the  $\alpha$  quantile.

Similarly, for a point estimate, since  $\theta$  may reside on a low-dimensional space  $\mathcal{M}$ , the sample mean of  $\theta$  or  $g(\theta)$  is not ideal as it may end up being high-dimensional. Therefore, we use the Fréchet mean:

$$\overline{g(\theta)} = \arg \min_{g(z): z \in \mathcal{M}} \mathbb{E}_{\theta \sim \pi(\theta|y)} \|g(z) - g(\theta)\|^2.$$

As we often do not know  $\mathcal{M}$ , we can approximate the above using the posterior samples  $\{\theta^j\}_{j=1\dots m}$ , which give the estimator  $\arg \min_{g(z): z \in \{\theta^j\}} \sum_{\theta \in \{\theta^j\}} \|g(z) - g(\theta)\|^2$ . We will illustrate these in the numerical examples.

## 6 Numerical Experiments

In this section, we use numeric experiments to illustrate the advantages of the  $l_1$ -ball prior. In all the examples, we use  $\beta_i \sim \text{DE}(0, \lambda_i)$ , with  $\lambda_i \sim \text{Exp}(\alpha_\lambda)$  ( $\alpha_\lambda = 1$  unless stated otherwise); the prior on the radius/threshold for  $\tilde{\mu}$  as described in section 2.3 with  $a_w = p$ ,  $b_w = 1$ , to reflect the prior belief that  $\theta$  or its transform should be very sparse.

### 6.1 Change Point Detection: Comparison with the Continuous Shrinkage Prior

As motivated early, a key strength of the  $l_1$ -ball prior is the ability of yielding exact zeros in the posterior. To show that the exact zeros are essential for the success of the  $l_1$ -tricks, we first experiment with a change point detection model and compare the results with the continuous shrinkage prior.

We use the simulated data with  $y_t \mid \mu_t \sim N(\mu_t, \sigma^2)$  for  $t = 1, \dots, 100$ , where  $\mu_t$  is piecewise constant from  $\{30, 10, 40, 20\}$  with three change points at  $t \in \{20, 40, 80\}$ . In order to compare with the continuous shrinkage prior, we re-parameterize this as a linear regression problem using



$\theta_t = \mu_t - \mu_{t-1}$ :

$$y_t = \sum_{i=1}^t \theta_i + \epsilon_t, \quad \epsilon_t \sim N(0, \sigma^2), \quad t = 1, \dots, 100,$$

where we use  $\sigma^2 = 10$  during the data generation. This enables us to impose sparsity on  $\theta_t$ , as the curve is a flat line in  $[t, t+d]$  if  $\theta_t = \theta_{t+1} = \dots = \theta_{t+d} = 0$ , and nonzero values only occur at the sudden changes. We use the  $l_1$ -ball prior on  $\theta_i$ ; to compare, we also test the model with a horseshoe prior on  $\theta_i$  [Carvalho et al., 2010]. In both cases, we use the Jeffreys' prior  $\pi_{\sigma^2}(\sigma^2) \propto 1/\sigma^2$

As shown in Figure 3 (c), under the  $l_1$ -ball prior, we obtain the posterior curves in step functions, as desired in this model. On the other hand, the horseshoe prior could not produce a step function, due to the small increments/decrements accumulate over time (e), leading to a clear departure from a step function curve.

To be fair, this is an expected result as the continuous shrinkage prior is not designed for handling such a problem. In fact, comparing Panels b and d, the horseshoe prior here has a good performance in the uncertainty quantification on each of  $\theta_i$ . However, a key difference is in the *joint* probability of all  $\theta_i$ 's — in this case, the horseshoe prior does not have a large probability for the neighboring  $\theta_i$ 's to have  $\sum_{i=t}^{t+d} |\theta_i| = 0$ ; whereas the  $l_1$ -ball does have this property, since all these small  $\beta_i$ 's with  $|\beta_i| \leq \tilde{\mu}$  are now reduced to exact zero.

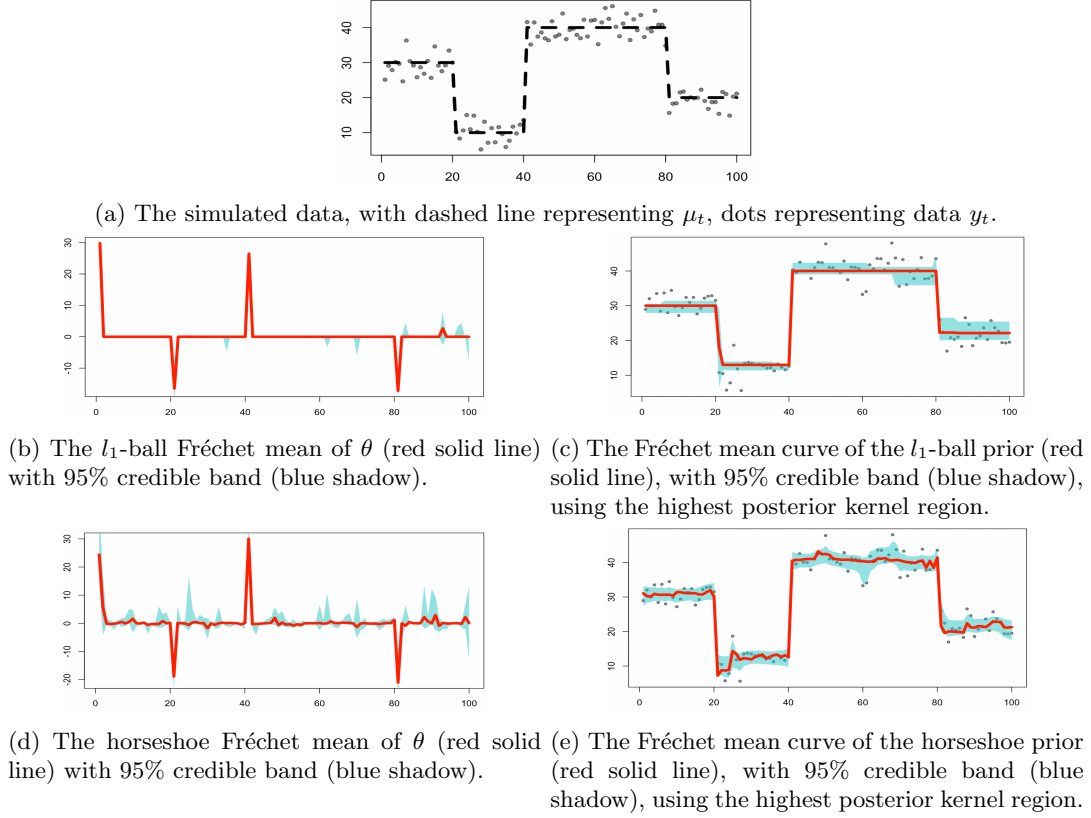


Figure 3: Comparing the performances of applying  $l_1$ -ball prior and continuous shrinkage prior in the change point detection model: the  $l_1$ -ball produces a step function with a few steps corresponding to the major changes, whereas the continuous shrinkage prior produces small increments/decrements that accumulate over time to a non-trivial departure from a step function.

## 6.2 Closed Probability Simplex for Finding the Number of Components

To illustrate the usefulness of exact zeros outside the linear models, we consider the prior specification problem for the finite mixture model. We focus on the  $K$ -component Gaussian mixture likelihood:

$$\pi(y_j; \theta, \mu, \sigma^2) = \sum_{k=1}^K \theta_k \phi(y_j \mid \mu_k, \sigma_k^2),$$

for  $j = 1, \dots, n$ , where  $\phi(\cdot \mid a, b)$  denotes the normal density with the mean  $a$  and variance  $b$ .

Suppose the data are generated from a  $K_0$ -component model, but we do not know  $K_0$  exactly; hence a common Bayesian modeling practice is to assign a prior on the  $\theta_k$ 's and shrink some of them close to zero. For example, it has been popular to use the infinite mixture model, which considers  $K$  as unbounded and assigns a stick-breaking construction on  $\{\theta_k\}_{k=1}^\infty$ , such as the one in the Dirichlet process. However, this was recently discovered to yield an inconsistent result [Miller and Harrison, 2014] for the number of components, as the posterior probability  $\text{pr}(K = K_0)$  goes to zero as  $n \rightarrow \infty$ . Later, Miller and Harrison [2018] show that instead of

putting a infinite mixture prior on  $\theta_k$ , if we treat  $K$  as finite number and put a prior  $\Pi_K(K)$ , this can yield a consistent estimation at  $K_0$ . They refer to it as the “mixture of finite mixtures” model. The major drawback is that this involves a combinatorial search over different  $K$ ’s.

Using the  $l_1$ -ball prior, we can significantly simplify this problem. Assuming we know a  $K_1$  large enough to have  $K_1 > K_0$ , starting from  $\beta_i \sim \text{DE}(0, \lambda_i)$ , we project it to the  $l_1$ -ball and apply the transformation:

$$w = P_{\mathbb{B}_r}(\beta), \quad \theta_k = \frac{|w_k|}{\sum_{i=1}^{K_1} |w_i|} \text{ for } k = 1, \dots, K_1,$$

note that in the second step, we have  $\sum_{i=1}^{K_1} |w_i| = r$  if  $\sum_{i=1}^{K_1} |\beta_i| \geq r$ . Compared to the parameter space in an infinite mixture model  $\{\theta : \theta_k > 0 \ \forall k \in \mathbb{Z}_+, \sum_{k=1}^{\infty} \theta_k = 1\}$ , besides being finite dimensional, a key difference here is that the space of  $\theta$  is the *closure* of the probability simplex (which includes the case for some  $\theta_k = 0$ ),

$$\Delta^{K_1-1} = \{\theta : \theta_k \geq 0 \ \forall k, \sum_{k=1}^{K_1} \theta_k = 1\},$$

Therefore, using the projection, we assign a positive probability for each  $K \in \{1, \dots, K_1\}$ ; hence this gives a continuous version of the mixture of finite mixtures model.

When simulating the data, we use  $K_0 = 3$  with  $(0.3, 0.3, 0.4)$  as the mixture weights; to have the components overlap, we use  $\mu_1 = 0, \mu_2 = 4, \mu_3 = 6$ , and all  $\sigma_1^2 = \sigma_2^2 = \sigma_3^2 = 1$ . We generate  $n = 1,000$  in the simulation.

For the  $l_1$ -ball prior, we use  $K_1 = 10$ , Inverse-Gamma(1, 1) prior for  $\sigma_k^2$  and  $N(0, 10^2)$  prior for  $\mu_k$ . To compare, we also use (i) the Dirichlet process mixture model with the concentration parameter  $\alpha = 1$ ; (ii) the finite mixture model with the same dimension  $K_1 = 10$ , but with a finite Dirichlet distribution prior  $(\theta_1, \dots, \theta_{K_1}) \sim \text{Dir}(\alpha)$  with  $\alpha = 0.001$  to favor sparsity in  $\theta$ . We use the same prior for  $\mu_k$  and  $\sigma_k^2$ .

Figure 4 shows the posterior distribution of  $K$  in all three models. Clearly, the one uses the  $l_1$ -ball has the largest probability assigned to  $K_0 = 3$ . Both the Dirichlet process mixture model and the finite mixture model with a Dirichlet prior put the largest probability at  $K = 4$ . These results are coherent with the theory finding. In addition, we compare the computing performance using the  $l_1$ -ball prior against the combinatorial search using the split-merge algorithm [Jain and Neal, 2007]. The  $l_1$ -ball mixture of finite mixtures enjoys faster mixing and less autocorrelation.

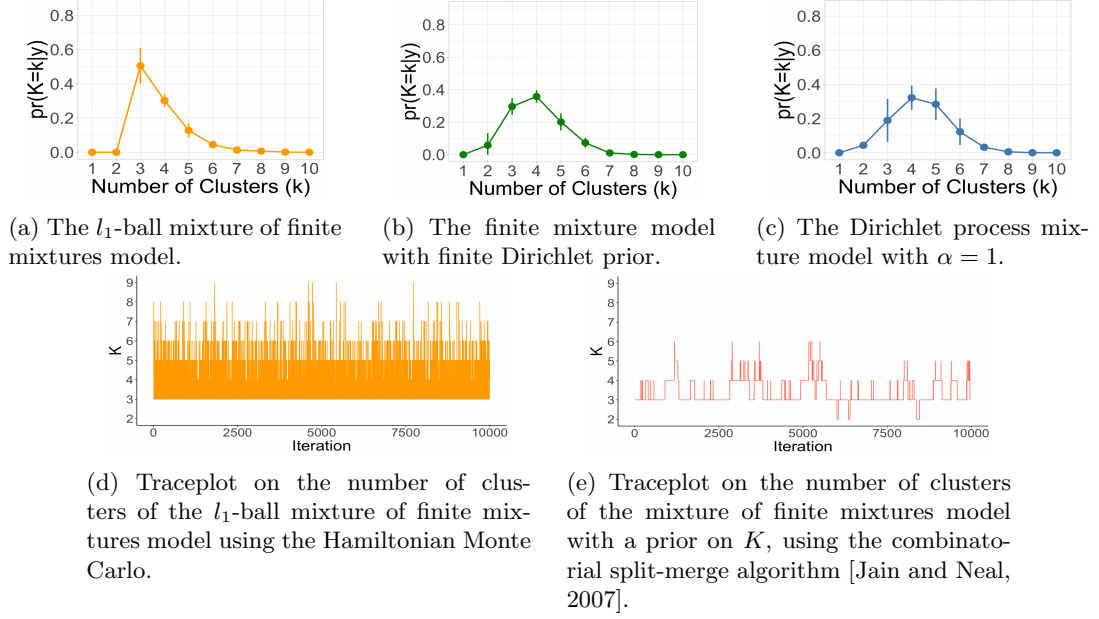


Figure 4: Comparing the performances of applying  $l_1$ -ball prior to the finite mixture weight and the other mixture models. The experiment is repeated five times, and the mean of the number of clusters with its standard error is presented. In each experiment, we run the Markov chain for 20,000 iterations and discard the first 10,000 as burn-ins.

## 7 Data Application: Sparse Change Detection in the Medical Images

For the application, we use the  $l_1$ -ball prior on the analysis of a medical imaging dataset. The data are the abdominal dynamic contrast-enhanced magnetic resonance imaging [Otazo et al., 2015], collected on a healthy human subject during normal breathing. It is in the form of a video, acquired via a whole-body scanner to record the aorta, portal vein and liver enhancement. There are  $384 \times 384$  pixels in each frame (corresponding to 0.94 seconds) and  $T = 75$  frames in total.

An important scientific task is to detect the locations of the large changes, corresponding to the important organ activities. However, there are a few challenges: (i) the most parts of the image are not fixed but also dynamically changing (such as the overall brightness, although to a less degree compared to the sharp changes), hence we need to model a “background” time series; (ii) the video is noisy hence there are uncertainties on the detected changes.

To handle this problem, we consider the low-rank plus sparse model:

$$M_t = \sum_{k=1}^d \alpha_{t,k} \psi_k + S_t + E_t,$$

for  $t = 1, \dots, T$ ; where the  $\psi_k \in \mathbb{R}^{384 \times 384}$  corresponds to some latent component shared by all frames, and  $\alpha_{t,k}$  is the loading dynamically changing over time;  $S_t \in \mathbb{R}^{384 \times 384}$  is a sparse matrix corresponding to the sharp changes that we wish to detect;  $E_t$  corresponds to the noise and we model it as independent  $N(0, \sigma_e^2)$  for each of its element.

A common problem for low-rank modeling is to determine the rank, in this case, the number of latent components  $d$ . Bhattacharya and Dunson [2011] previously proposed to view  $d$  as unbounded, while applying a continuous shrinkage prior on the scale of loading, closer towards zero as  $k$  increases. We are inspired by this idea, nevertheless, we achieve an exact rank selection by using a generalized  $l_1$ -ball prior based on the nuclear norm. This has two advantages: we can treat the low-rank part using one matrix parameter  $L$  replacing  $\sum_k \alpha_{t,k} \psi_k$ , which avoids the potential identifiability issues when estimating  $\alpha_{t,k}$  and  $\psi_k$  separately; having an exactly low-rank part reduces the confoundingness between the near-low-rank and sparse signals.

Specifically, we reparameterize the 75 matrices  $\{\sum_{k=1}^d \alpha_{t,k} \psi_k\}_{t=1}^T$  via a single matrix of size  $75 \times 384^2$ :

$$L = \sum_{k=1}^d (\alpha_{1,k}, \dots, \alpha_{T,k}) [\text{vec}(\psi_k)]^T.$$

Without specifying  $d$ , we can treat  $L$  as the output of projecting a dense matrix  $\beta \in \mathbb{R}^{75 \times 384^2}$  to a generalized  $l_1$ -ball:

$$L = \underset{Z \in \mathbb{R}^{75 \times 384^2} : \|Z\|_* \leq r}{\text{argmin}} \|Z - \beta\|_F^2$$

where  $\|Z\|_*$  denotes the nuclear norm, as the sum of the singular values  $\sum_{k=1}^{75} \rho_k(Z)$ , with  $Z = U_Z \text{diag}[\rho_k(Z)] V_Z^T$ . Since having exact  $\rho_k(Z) = 0$  for some  $k$ 's will lead to an effective rank reduction to  $d = |\{\rho_k(Z) : \rho_k(Z) > 0\}|$ , the nuclear norm regularization is very popular in the optimization literature [Hu et al., 2012]. This projection has a closed-form solution: if  $\sum_k \rho_k(\beta) \geq r$ ,  $L = U_\beta \text{diag}[(\rho_k(\beta) - \tilde{\mu})_+] V_\beta^T$ , for some  $\tilde{\mu} > 0$  such that  $\sum_k [\rho_k(\beta) - \tilde{\mu}]_+ = r$ ;  $L = \beta$  if  $\sum_k \rho_k < r$ .

Assigning  $\beta_{i,j} \sim \text{DE}(0, \lambda_{i,j})$ , we can quantify the uncertainty regarding the rank. Further, we assign the elementwise  $l_1$ -ball prior on each element of  $S_t$ , so that we can obtain sparse estimates on the sharp changes.

Figure 5 shows that the background time series is mostly based on the linear combination of 2 latent components (panel a), each corresponds to a dense image (b-c). By visualizing the estimated backgrounds at three different time points, we can see some very subtle differences, such as the brightness between (d) and (f), which involves most of the pixels. Indeed, these small changes are what we wish to find and separate from the sparse part  $S_t$ .

Figure 6 shows the locations of the sharp changes we estimate from the sparse  $S_t$ . The results are very interpretable as they correspond to when the aorta, portal vein and liver are in their enhancement phases, respectively. The vessels and organs are distinct from the abdominal background. Further, we compute the pixel-wise variance for these sparse estimates, as a measurement of the uncertainty. It can be seen that the aorta and portal vein (panels g and h) have a relatively low uncertainty on the changes; whereas the liver (panel i) has a higher uncertainty, hence some caution should be applied when making conclusion based on the last frame.

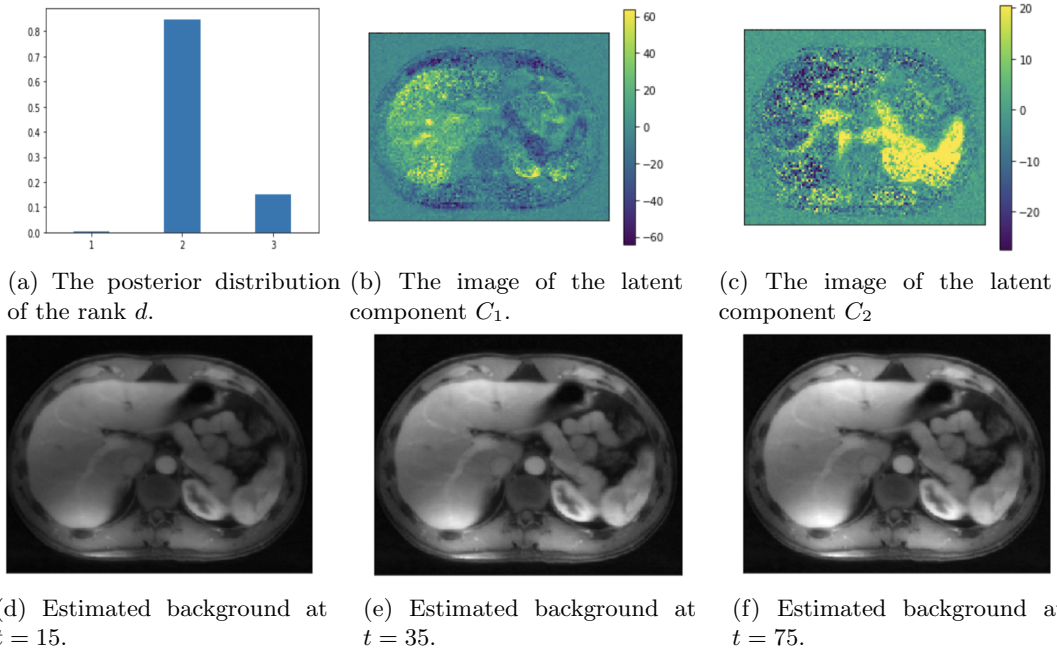


Figure 5: The low-rank modeling of the video background  $L$ , where  $L$  is a flattened matrix containing all the background images over 75 time points. The posterior distribution is concentrated at a low rank  $d = 2$  for the matrix  $L$  (panel a). This captures the subtle changes that happen in the background, such as the brightness between (d) and (f).

In addition, we experiment with a simpler alternative that replaces the low-rank  $\sum_{k=1}^d \alpha_{t,k} \psi_k$  with a time-invariant background  $\psi_0$ . This leads to much less sparse estimates about the locations, that are more difficult to interpret. We provide the results in the appendix.

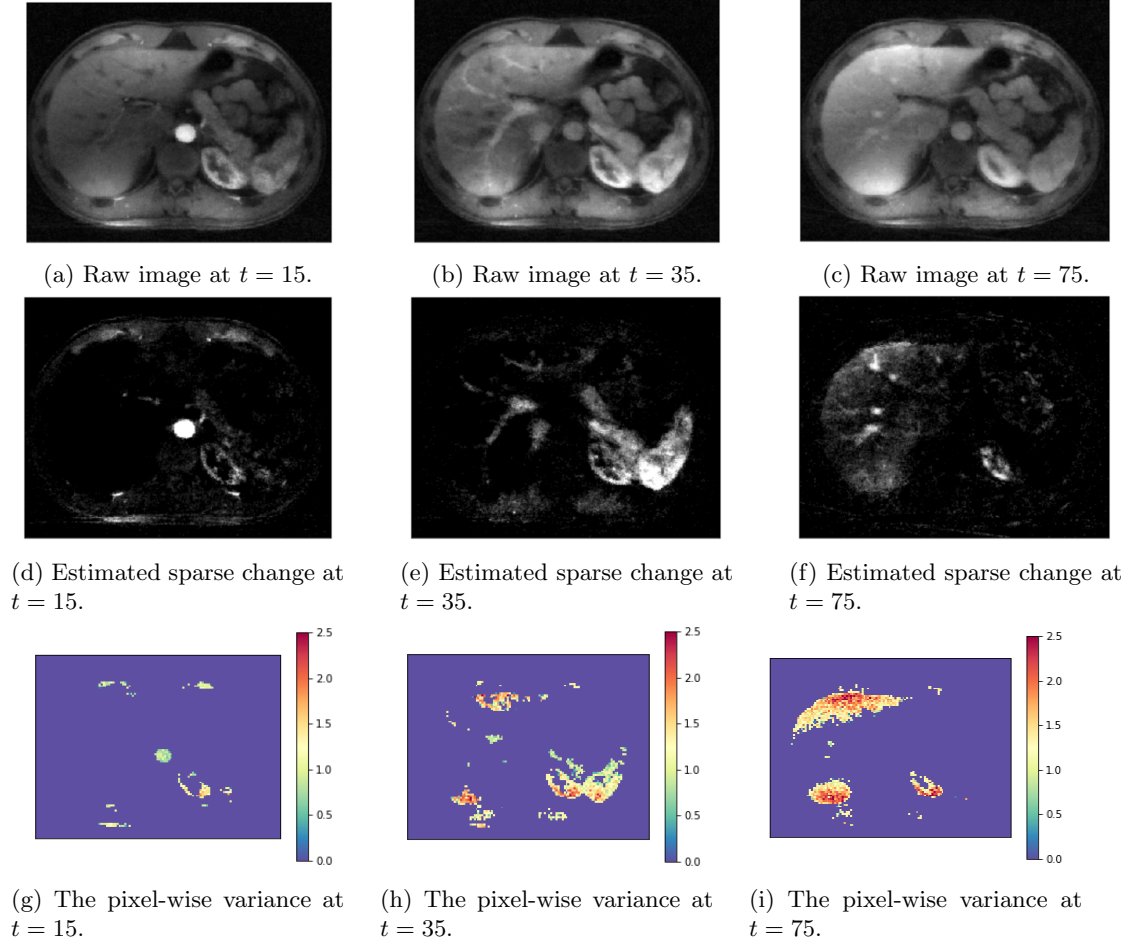


Figure 6: The sparse change component  $S_t$  and its pixel-wise variances are visualized. The three frames correspond to three time points, when aorta, liver and portal vein are in their enhancement phase respectively. The posterior of the sparse parameter shows the locations of these changes, as well as the uncertainties.

## 8 Discussion

In this article, we propose a new prior defined on the boundary of the  $l_1$ -ball. This allows us to build many interesting applications that implicitly involves a combinatorial selection, such as in the change points, the number of mixture components and the rank of a matrix. We show that the  $l_1$ -ball projection is continuous hence giving a convenient “continuous embedding” for these combinatorial problems, establishing a connection between the rich optimization and Bayesian literature.

There are several interesting extensions worth pursuing. First, as we observed, when projecting a continuous distribution into the boundary of a certain geometric set, it often leads to a degenerate distribution that is useful but difficult to parameterize directly. This convenient property is not limited to the  $l_1$ -ball. For example, in the high-dimensional optimal transport problem, when estimating the contingency probability table given two marginal probability vec-

tors, the solution table is likely to be very sparse [Cuturi, 2013]. This is due to the projection to the high-dimensional polytope will likely end up in the vertex corresponding to a high sparsity. Therefore, our projection idea can be generalized to such useful geometric sets. Second, the data augmentation strategy developed in this article can be viewed as “augmentation-by-optimization”, as opposed to the conventional “augmentation-by-integration”. Polson and Scott [2016] have previously explored the connection and difference between maximizing and integrating over a latent variable, under the scope of comparing a frequentist/optimization-based model and its Bayesian counterpart; here, we demonstrate that the barrier can be in fact removed, and the Bayesian models can leverage a maximization over a certain latent variable, creating a new class of useful priors. The use of optimization techniques for the Bayesian approach has recently become popular, especially with a computational focus, such as the proximal Markov chain Monte Carlo [Pereyra, 2016]; on the other hand, our method shows that one could use such a technique for the purpose of model/prior building. Clearly, there is a large pool of optimization tricks and geometric objects that one can further exploit.

## References

- Artin Armagan, David B Dunson, and Jaeyong Lee. Generalized Double Pareto Shrinkage. *Statistica Sinica*, 23(1):119, 2013.
- Ray Bai and Malay Ghosh. On the Beta Prime Prior for Scale Parameters in High-Dimensional Bayesian Regression Models. *Statistica Sinica*, 2019.
- Amir Beck. *First-order Methods in Optimization*. SIAM, 2017.
- Anirban Bhattacharya and David B Dunson. Sparse Bayesian Infinite Factor Models. *Biometrika*, pages 291–306, 2011.
- Anirban Bhattacharya, Debdeep Pati, Natesh S Pillai, and David B Dunson. Dirichlet–Laplace Priors for Optimal Shrinkage. *Journal of the American Statistical Association*, 110(512):1479–1490, 2015.
- Anirban Bhattacharya, Antik Chakraborty, and Bani K Mallick. Fast Sampling With Gaussian Scale Mixture Priors in High-Dimensional Regression. *Biometrika*, page asw042, 2016.
- Stephen Boyd, Neal Parikh, and Eric Chu. *Distributed Optimization and Statistical Learning via the Alternating Direction Method of Multipliers*. Now Publishers Inc, 2011.
- M Breth et al. Bayesian Confidence Bands for a Distribution Function. *The Annals of Statistics*, 6(3):649–657, 1978.
- Peter Bühlmann and Sara Van De Geer. *Statistics for High-dimensional Data: Methods, Theory and Applications*. Springer Science & Business Media, 2011.
- Carlos M Carvalho, Nicholas G Polson, and James G Scott. The Horseshoe Estimator for Sparse Signals. *Biometrika*, 97(2):465–480, 2010.
- Ismaël Castillo and Aad van der Vaart. Needles and Straw in a Haystack: Posterior Concentration for Possibly Sparse Sequences. *The Annals of Statistics*, 40(4):2069–2101, 2012.
- Ismaël Castillo, Johannes Schmidt-Hieber, and Aad Van der Vaart. Bayesian Linear Regression with Sparse Priors. *The Annals of Statistics*, 43(5):1986–2018, 2015.



- Scott Shaobing Chen, David L Donoho, and Michael A Saunders. Atomic Decomposition by Basis Pursuit. *SIAM Review*, 43(1):129–159, 2001.
- Marco Cuturi. Sinkhorn Distances: Lightspeed Computation of Optimal Transport. *Advances in Neural Information Processing Systems*, 26:2292–2300, 2013.
- John Duchi, Shai Shalev-Shwartz, Yoram Singer, and Tushar Chandra. Efficient Projections onto the  $L_1$ -Ball for Learning in High Dimensions. In *Proceedings of the 25th International Conference on Machine Learning*, pages 272–279, 2008.
- Bradley Efron, Trevor Hastie, Iain Johnstone, and Robert Tibshirani. Least Angle Regression. *The Annals of Statistics*, 32(2):407–499, 2004.
- Jianqing Fan, Han Liu, Yang Ning, and Hui Zou. High Dimensional Semiparametric Latent Graphical Model for Mixed Data. *Journal of the Royal Statistical Society: Series B (Statistical Methodology)*, 79(2):405–421, 2017.
- Herbert Federer. *Geometric Measure Theory*. Springer, 2014.
- Edouard Grave, Guillaume R Obozinski, and Francis R Bach. Trace Lasso: a Trace Norm Regularization for Correlated Designs. In *Advances in Neural Information Processing Systems*, pages 2187–2195, 2011.
- Laura H Gunn and David B Dunson. A Transformation Approach for Incorporating Monotone or Unimodal Constraints. *Biostatistics*, 6(3):434–449, 2005.
- Matthew D Hoffman and Andrew Gelman. The No-U-Turn Sampler: Adaptively Setting Path Lengths in Hamiltonian Monte Carlo. *Journal of Machine Learning Research*, 15(1):1593–1623, 2014.
- Yao Hu, Debing Zhang, Jieping Ye, Xuelong Li, and Xiaofei He. Fast and Accurate Matrix Completion via Truncated Nuclear Norm Regularization. *IEEE transactions on pattern analysis and machine intelligence*, 35(9):2117–2130, 2012.
- Sonia Jain and Radford M Neal. Splitting and Merging Components of a Nonconjugate Dirichlet Process Mixture Model. *Bayesian Analysis*, 2(3):445–472, 2007.
- Michael Jauch, Peter D Hoff, and David B Dunson. Monte Carlo Simulation on the Stiefel Manifold via Polar Expansion. *Journal of Computational and Graphical Statistics*, pages 1–23, 2020.
- Lizhen Lin and David B Dunson. Bayesian Monotone Regression Using Gaussian Process Projection. *Biometrika*, 101(2):303–317, 2014.
- Fredrik Lindsten, Henrik Ohlsson, and Lennart Ljung. Clustering Using Sum-of-norms Regularization: With Application to Particle Filter Output Computation. In *2011 IEEE Statistical Signal Processing Workshop (SSP)*, pages 201–204. IEEE, 2011.
- Nicolai Meinshausen and Peter Bühlmann. High-dimensional Graphs and Variable Selection with the Lasso. *The Annals of Statistics*, 34(3):1436–1462, 2006.
- Jeffrey W Miller and Matthew T Harrison. Inconsistency of Pitman-Yor Process Mixtures for the Number of Components. *Journal of Machine Learning Research*, 15(1):3333–3370, 2014.

- Jeffrey W Miller and Matthew T Harrison. Mixture Models with a Prior on the Number of Components. *Journal of the American Statistical Association*, 113(521):340–356, 2018.
- Toby J Mitchell and John J Beauchamp. Bayesian Variable Selection in Linear Regression. *Journal of the American Statistical Association*, 83(404):1023–1032, 1988.
- Radford M. Neal. MCMC using Hamiltonian Dynamics. In Steve Brooks, Andrew Gelman, Galin Jones, and Xiao-Li Meng, editors, *Handbook of Markov Chain Monte Carlo*, chapter 5. CRC Press, 2011.
- Akihiko Nishimura, David B Dunson, and Jianfeng Lu. Discontinuous Hamiltonian Monte Carlo for Discrete Parameters and Discontinuous Likelihoods. *Biometrika*, 107(2):365–380, 2020.
- Ricardo Otazo, Emmanuel Candes, and Daniel K Sodickson. Low-Rank Plus Sparse Matrix Decomposition for Accelerated Dynamic MRI With Separation of Background and Dynamic Components. *Magnetic Resonance in Medicine*, 73(3):1125–1136, 2015.
- Ari Pakman and Liam Paninski. Auxiliary-variable Exact Hamiltonian Monte Carlo Samplers for Binary Distributions. *arXiv preprint arXiv:1311.2166*, 2013.
- Trevor Park and George Casella. The Bayesian Lasso. *Journal of the American Statistical Association*, 103(482):681–686, 2008.
- Marcelo Pereyra. Proximal Markov Chain Monte Carlo Algorithms. *Statistics and Computing*, 26(4):745–760, 2016.
- Nicholas G Polson and James G Scott. Mixtures, Envelopes and Hierarchical Duality. *Journal of the Royal Statistical Society: Series B: Statistical Methodology*, pages 701–727, 2016.
- Veronika Ročková and Edward I George. The Spike-and-slab Lasso. *Journal of the American Statistical Association*, 113(521):431–444, 2018.
- Deborshee Sen, Sayan Patra, and David Dunson. Constrained Inference Through Posterior Projections. *arXiv preprint arXiv:1812.05741*, 2018.
- Ali Shojaie and George Michailidis. Penalized Likelihood Methods for Estimation of Sparse High-dimensional Directed Acyclic Graphs. *Biometrika*, 97(3):519–538, 2010.
- Kean Ming Tan and Daniela Witten. Statistical Properties of Convex Clustering. *Electronic Journal of Statistics*, 9(2):2324, 2015.
- Martin A Tanner and Wing Hung Wong. The Calculation of Posterior Distributions by Data Augmentation. *Journal of the American Statistical Association*, 82(398):528–540, 1987.
- Robert Tibshirani. Regression Shrinkage and Selection via the Lasso. *Journal of the Royal Statistical Society: Series B (Statistical Methodology)*, 58(1):267–288, 1996.
- Robert Tibshirani, Michael Saunders, Saharon Rosset, Ji Zhu, and Keith Knight. Sparsity and Smoothness via the Fused Lasso. *Journal of the Royal Statistical Society: Series B (Statistical Methodology)*, 67(1):91–108, 2005.
- Roman Vershynin. *High-dimensional Probability: An Introduction with Applications in Data Science*, volume 47. Cambridge University Press, 2018.
- Ming Yuan and Yi Lin. Model Selection and Estimation in Regression with Grouped Variables. *Journal of the Royal Statistical Society: Series B (Statistical Methodology)*, 68(1):49–67, 2006.

Teng Zhang and Hui Zou. Sparse Precision Matrix Estimation via Lasso Penalized D-trace Loss. *Biometrika*, 101(1):103–120, 2014.

Hui Zou and Trevor Hastie. Regularization and Variable Selection via the Elastic Net. *Journal of the Royal Statistical Society: Series B (Statistical Methodology)*, 67(2):301–320, 2005.

Hui Zou, Trevor Hastie, and Robert Tibshirani. Sparse Principal Component Analysis. *Journal of Computational and Graphical Statistics*, 15(2):265–286, 2006.

## Appendix

### Proof of Theorem 1

*Proof.* Since permutation of indices does not affect  $|J|$ , without loss of generality, we assume  $\sum_{i=1}^c |\theta_i| = r$  and  $|\theta_i| > 0$  for  $i = 1, \dots, c$ .

Now  $f^{-1}$  is a mapping from  $(\theta_1, \dots, \theta_{c-1}, t_{c+1}, \dots, t_p, \mu)$  to  $(\beta_1, \dots, \beta_{c-1}, \beta_{c+1}, \dots, \beta_p, \beta_c)$ , where  $\beta_c = s_c(r - \sum_{i=1}^{c-1} |\theta_i| + \mu/c)$ . The Jacobian matrix  $J$  is

$\frac{\partial}{\partial \theta_1}$	$\beta_1$	$\cdots$	$\beta_{c-1}$	$\beta_{c+1}$	$\cdots$	$\beta_p$	$\beta_c$
$\vdots$	$\vdots$	$\ddots$	$\vdots$	$\vdots$	$\vdots$	$\vdots$	$\vdots$
$\frac{\partial}{\partial \theta_{c-1}}$	0	$\cdots$	1	0	$\vdots$	0	$-s_{c-1}s_c$
$\frac{\partial}{\partial t_{c+1}}$	0		0	$s_{c+1}$	0	0	0
$\vdots$	$\vdots$	$\vdots$	$\vdots$	$\vdots$	$\ddots$	$\vdots$	$\vdots$
$\frac{\partial}{\partial t_p}$	0	$\cdots$	0	0	$\cdots$	$s_p$	0
$\frac{\partial}{\partial \mu}$	$s_1/c$	$\cdots$	$s_{c-1}/c$	$s_{c+1}/c$	$\cdots$	$s_p/c$	$s_c/c$

Split the matrix into four blocks, with  $A = J_{1:(p-1), 1:(p-1)}$ ,  $B = J_{p, 1:(p-1)}$ ,  $C = J_{1:(p-1), p}$  and  $D = s_c/c$ . We know

$$\begin{aligned}
 |J| &= |D - BA^{-1}C||A| \\
 &= |s_c/c + \sum_{i=1}^{c-1} s_i^2 s_c/c| \times 1 \\
 &= |s_c| \\
 &= 1.
 \end{aligned}$$

□

### Proof of Theorem 2

*Proof.* With  $\beta_i$ 's re-ordered  $|\beta_{(1)}| \geq \dots \geq |\beta_{(p)}|$ , we will prove  $|\beta_{(j)}| > (\sum_{i=1}^j |\beta_{(i)}| - r)/j$  for all  $j \leq |C|$  and  $|\beta_{(j)}| < (\sum_{i=1}^j |\beta_{(i)}| - r)/j$  for  $j > |C|$ . This is equivalent to comparing  $(j-1)|\beta_{(j)}| - (\sum_{i=1}^{j-1} |\beta_{(i)}| - r)$  against 0.

When  $j \leq |C|$ ,

$$\begin{aligned}
& (j-1)|\beta_{(j)}| - \left(\sum_{i=1}^{j-1} |\beta_{(i)}| - r\right) \\
&= (j-1)\left(|\theta_{(j)}| + \frac{\mu}{|C|}\right) - \left\{\sum_{i=1}^{j-1} \left(|\theta_{(i)}| + \frac{\mu}{|C|}\right) - r\right\} \\
&= (j-1)|\theta_{(j)}| - \left(\sum_{i=1}^{j-1} |\theta_{(i)}| - r\right) \\
&> 0,
\end{aligned}$$

since  $\sum_{i=1}^{j-1} |\theta_{(i)}| < r$  for  $j \leq |C|$ .

When  $j > |C| + 1$ ,

$$\begin{aligned}
& (j-1)|\beta_{(j)}| - \left(\sum_{i=1}^{j-1} |\beta_{(i)}| - r\right) \\
&= (j-1)\left(t_{(j)} + \frac{\mu}{|C|}\right) - \left\{\sum_{i=1}^{|C|} \left(|\theta_{(i)}| + \frac{\mu}{|C|}\right) + \sum_{i=|C|+1}^{j-1} \left(t_{(i)} + \frac{\mu}{|C|}\right) - r\right\} \\
&= (j-1)t_{(j)} - \left\{\sum_{i=1}^{|C|} |\theta_{(i)}| + \sum_{i=|C|+1}^{j-1} t_{(i)} - r\right\} \\
&\stackrel{(a)}{=} (j-1)t_{(j)} - \sum_{i=|C|+1}^{j-1} t_{(i)} \\
&\stackrel{(b)}{<} (j-1-|C|)t_{(j)} - \sum_{i=|C|+1}^{j-1} t_{(i)} \\
&= \sum_{i=|C|+1}^{j-1} (t_{(j)} - t_{(i)}) \\
&\stackrel{(c)}{\leq} 0,
\end{aligned}$$

where (a) is due to  $\sum_{i=1}^{|C|} |\theta_{(i)}| = r$ , (b) due to  $t_{(j)} < 0$  and (c) due to  $|\beta_{(j)}| - \mu/|C| \leq |\beta_{(i)}| - \mu/|C|$  for  $j > i$ .

When  $j = |C| + 1$ ,  $(j-1)|\beta_{(j)}| - (\sum_{i=1}^{j-1} |\beta_{(i)}| - r) = |C|t_{(j)} < 0$ .

Therefore, we have  $c = |C|$ , and it can be verified that

$$\mu_c = \sum_{i=1}^{|C|} \left(|\theta_{(i)}| + \frac{\mu}{|C|}\right) - r = \mu.$$

□

### Proof of Theorem 3

*Proof.* For ease of notation, we denote  $\vec{t}_{\bar{C}} := t_{\sigma_1}, \dots, t_{\sigma_{p-|C|}}$

$$\begin{aligned}
\pi_\theta(\theta) &= \sum_{\substack{s_{\sigma_1}, \dots, s_{\sigma_{p-|C|}} \\ \in \{-1, 1\}^{p-|C|}}} \int_0^\infty \int_{(-\mu/|C|, 0)^{p-|C|}} \pi_\beta\{g(t, s, \mu)\} d\vec{t}_{\bar{C}} d\mu \\
&= 2^{p-|C|} (2\lambda)^{-p} \int_0^\infty \int_{(-\mu/|C|, 0)^{p-|C|}} \prod_{i \in C} \left\{ e^{-\frac{|\theta_i| + \mu/|C|}{\lambda}} \right\} \prod_{i \in \bar{C}} \left\{ e^{-\frac{t_i + \mu/|C|}{\lambda}} \right\} d\vec{t}_{\bar{C}} d\mu \\
&= 2^{p-|C|} (2\lambda)^{-p} \prod_{i \in C} \left\{ \exp\left(-\frac{|\theta_i|}{\lambda}\right) \right\} \int_0^\infty e^{-\frac{p\mu}{\lambda|C|}} \int_{(-\mu/|C|, 0)^{p-|C|}} \prod_{i \in \bar{C}} e^{-\frac{t_i}{\lambda}} d\vec{t}_{\bar{C}} d\mu \\
&= 2^{p-|C|} (2\lambda)^{-p} \exp\left(-\frac{r}{\lambda}\right) \cdot \lambda^{p-|C|} \int_0^\infty e^{-\frac{p\mu}{\lambda|C|}} \left(e^{\frac{\mu}{\lambda|C|}} - 1\right)^{p-|C|} d\mu.
\end{aligned}$$

Let  $u = e^{-\frac{\mu}{\lambda|C|}}$ , then  $du = -(\lambda|C|)^{-1} e^{-\frac{\mu}{\lambda|C|}} d\mu$ , we have

$$\int_0^\infty e^{-\frac{p\mu}{\lambda|C|}} \left(e^{\frac{\mu}{\lambda|C|}} - 1\right)^{p-|C|} d\mu = \lambda|C| \int_0^1 u^{|C|-1} (1-u)^{p-|C|} du = \lambda \frac{\Gamma(|C|+1)\Gamma(p-|C|+1)}{\Gamma(p+1)}.$$

Combining the results,

$$\pi_0(\theta) = \frac{(2\lambda)^{-|C|}}{\binom{p}{|C|}} \lambda \exp\left(-\frac{r}{\lambda}\right)$$

□

### Proof of Corollary 1

*Proof.* We first focus on when  $\|\theta\|_1 < r$ , since under which,  $|C| < p$  happens with probability zero, therefore,

$$\begin{aligned}
\text{pr}(|C| = p, \|\theta\|_1 < r) &= \int_{\mathbb{R}^p} \prod_i (2\lambda)^{-1} \exp(-|\theta_i|/\lambda) \mathbb{I}(\|\theta\|_1 < r) d\theta \\
&= \int_{\mathbb{R}_+^p} \prod_i (\lambda)^{-1} \exp(-x_i/\lambda) \mathbb{I}(\sum x_i < r) dx \\
&\stackrel{(a)}{=} \int_0^r \frac{1}{\Gamma(p)\lambda^p} y^{p-1} \exp(-y/\lambda) dy \\
&\stackrel{(b)}{=} 1 - \sum_{j=0}^{p-1} \frac{1}{j!} \left(\frac{r}{\lambda}\right)^j \exp(-r/\lambda),
\end{aligned}$$

where (a) uses the fact that sum of  $p$  iid  $\text{Exp}(\lambda)$ 's is a  $\text{Gamma}(p, \lambda)$ , and (b) uses the CDF formula as  $p$  is an integer.

When  $\|\theta\|_1 = r$ , and  $|C| = j$ , denote the non-zero indices by  $\{i_1, \dots, i_j\}$ , note that  $x = (|\theta_{i_1}|/r, \dots, |\theta_{i_j}|/r)$  is on a probability simplex with dimension  $(j-1)$ ,  $\Delta^{j-1}$ , hence we can use

Dirichlet distribution integral  $\int_{\Delta^{j-1}} 1dx = 1/\Gamma(j)$ . We have

$$\begin{aligned} \text{pr}(|C| = j, \|\theta\|_1 = r) &= \frac{(2\lambda)^{-j}}{\binom{p}{j}} \lambda \exp\left(-\frac{r}{\lambda}\right) 2^j \binom{p}{j} r^{j-1} / \Gamma(j) \\ &= \left(\frac{r}{\lambda}\right)^{j-1} \exp\left(-\frac{r}{\lambda}\right) / (j-1)!, \end{aligned}$$

for  $j = 1, \dots, p$ . Combining the above gives the result.  $\square$

## Proof of Theorem 4

*Proof.* The compatibility numbers are

$$\begin{aligned} \phi(C) &= \inf_{\beta} \left\{ \frac{\|X\beta\|_2 |C|^{1/2}}{\|X\|_{2,\infty} \|\beta_C\|_1} : \|\beta_{[p]\setminus C}\|_1 \leq 7 \|\beta_C\|_1, \beta_C \neq 0 \right\}, \\ \psi(C) &= \tilde{\phi} \left[ \left( 2 + \frac{3}{a+b} + \frac{33}{\phi(C)^2} \frac{\lambda^*}{2\|X\|_{2,\infty} \sqrt{\log p}} \right) |C| \right], \\ \tilde{\phi}(c) &:= \inf \left\{ \frac{\|X\theta\|_2}{\|X\|_{2,\infty} \|\theta\|_2} : 0 \neq |C_\theta| \leq c \right\}. \end{aligned}$$

Our results are based on the early work of Castillo et al. [2015], Theorems 1 and 2: For a constant  $\lambda^*$  and a discrete distribution  $g(c)$  supported on  $\{0, \dots, p\}$ , when

1.  $\|X\|_{2,\infty}/p \leq \lambda^* \leq 4\|X\|_{2,\infty} \sqrt{\log p}$ ,
2. There exist constants  $a_1, a_2, a_3, a_4 > 0$  with (2.2)  $a_1 p^{-a_3} \leq \frac{g(c)}{g(c-1)} \leq a_2 p^{-a_4}$  for  $c = 2, \dots, p$ .

Then for a prior kernel of the form

$$\pi_0(\theta; \lambda^*, g) = g(|C|) \frac{1}{\binom{p}{|C|}} \left(\frac{\lambda^*}{2}\right)^{|C|} \exp(-\lambda^* \|\theta\|_1),$$

with  $g(|C| = j) = \text{pr}(|C| = j)$ , would enjoy the results in the theorem. We now check these two conditions and compute the associated constants.

Using the chosen  $\lambda$  and  $\alpha$ , we have

$$\lambda^* = \frac{\lambda + \alpha}{\lambda \alpha} = \|X\|_{2,\infty} \frac{b_1 p^{b_2} + p^{b_3}}{b_1 p^{b_2} p^{b_3}},$$

Since  $b_3 \leq 1$ , we have  $\lambda^* \geq \|X\|_{2,\infty}/p^{b_3} \geq \|X\|_{2,\infty}/p$ . Since  $b_2 > b_3$ , for  $p$  large enough,  $b_1 p^{b_2} > p^{b_3}$ , hence  $\|X\|_{2,\infty} (b_1 p^{b_2} + p^{b_3}) / (b_1 p^{b_2} p^{b_3}) \leq 2/p^{b_3} \|X\|_{2,\infty} \leq 4\|X\|_{2,\infty} \sqrt{\log p}$ .

On the other hand, When  $c = 1, \dots, p-1$ .

$$\frac{g(c)}{g(c-1)} = (1 + \lambda/\alpha)^{-1} = \frac{1}{1 + b_1 p^{b_2 - b_3}}.$$

Clearly,  $g(c)/g(c-1) \leq 1/(b_1 p^{b_2 - b_3})$ , satisfying  $a_2 = 1/b_1$  and  $a_4 = b_2 - b_3$ . For  $p$  large enough  $b_1 p^{b_2 - b_3} > 1$ , we have  $g(c)/g(c-1) \geq 1/(2b_1 p^{b_2 - b_3})$ , satisfying  $a_1 = 1/(2b_1)$  and  $a_3 = b_2 - b_3$ . When  $c = p$ ,  $g(c)/g(c-1) = \alpha/\lambda = 1/(b_1 p^{b_2 - b_3})$ , hence also satisfying the above results. Therefore, we apply  $a_4 = b_2 - b_3$  in the two theorems of Castillo et al. [2015], and arrive at our results.  $\square$

## Simulation in Linear Regression

As discussed in the theory section, in the linear regression, the recovery of  $\theta^0$  requires some conditions on the cardinality of the true parameter  $c_0$ , and the sample size  $n$ . We now use numerical simulations to empirically estimate the sparsity detection limits and the required minimum sample size.

For each experiment setting, the  $n$  rows of the design matrix  $X \in \mathbb{R}^{n \times p}$  are independently drawn from  $N(0, I_p)$ . We generate the true  $\theta^0$  according to the level of sparsity, where the non-zero entries are drawn from  $N(5, 1)$ . We experiment with  $p = 200, 300, 500$  and  $800$ , with  $n$  being a multiple of  $p$  and  $c_0$  set to 25, 50, 75, 100, 150, 200 times  $\sqrt{1/\log p}$ , as corresponding to different degrees of sparsity. To be consistent with theory result on regression, we benchmark the the sup-norm  $\sup_i \|\hat{\theta}_i - \theta_i^0\|$  between the posterior mean  $\hat{\theta}$  and the oracle  $\theta^0$ . We plot the results in Figure 7, and make a few observations: (i) when  $n \geq p$ , all settings have low estimation errors close to zero; (ii) when  $n < p$ , we have good result roughly when  $c_0 \leq 2\sqrt{n/\log p}$ . This range is coherent with our theoretic analysis.

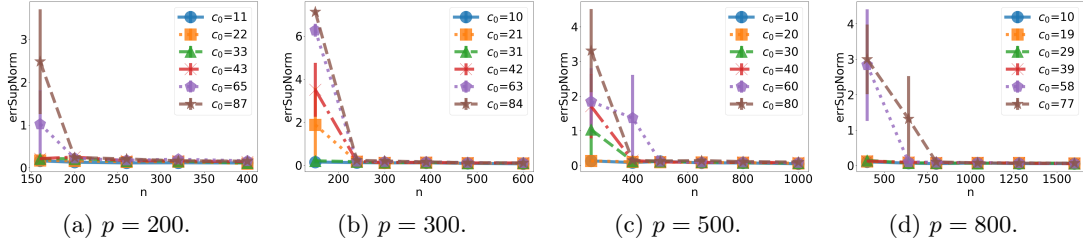


Figure 7: The simulation in sparse regression shows the  $l_1$ -ball prior can correctly recover  $\theta^0$  in  $l_\infty$  norm when  $c_0 \lesssim 2\sqrt{n/\log p}$ .

Next, we compare the performance of the  $l_1$ -ball prior with the Bayesian lasso and horseshoe priors, over a range of different  $p$ ,  $n$  and  $c_0$ . We now benchmark using the canonical regression settings for two Bayesian continuous priors: the horseshoe [Carvalho et al., 2010] and the Bayesian lasso [Park and Casella, 2008], implemented through R packages `monomvn` and `horseshoe` in regression problem. Specifically, in the model  $y_i = x_i^T \theta + \epsilon_i$ , with  $X \in \mathbb{R}^{n \times p}$  and  $\epsilon_i$  from  $N(0, 1)$ . We fix  $n = 200$  and consider  $p = 200$  and  $500$ . For each  $p$ , we let the true cardinality to be  $c_0 = 5, 10$  and  $20$ .

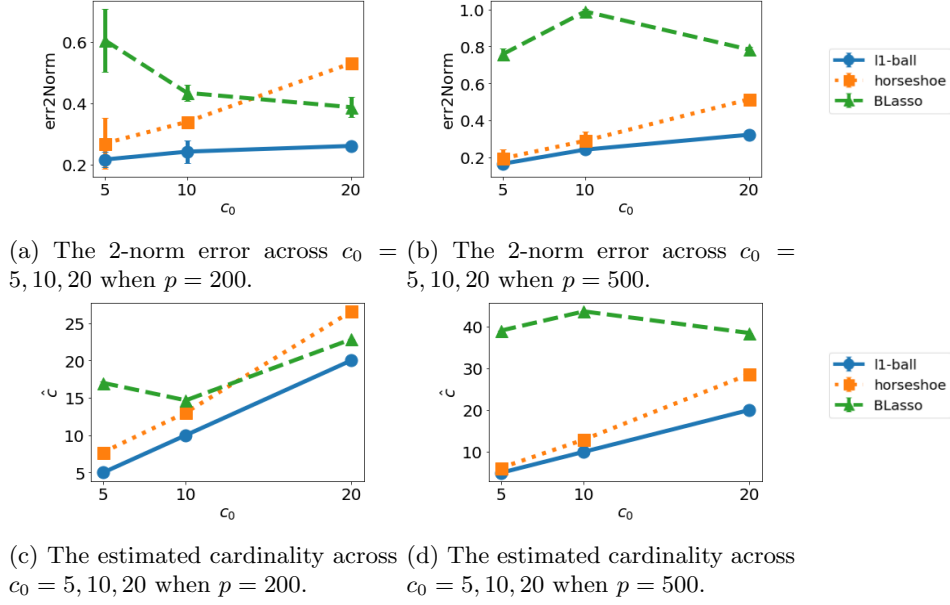
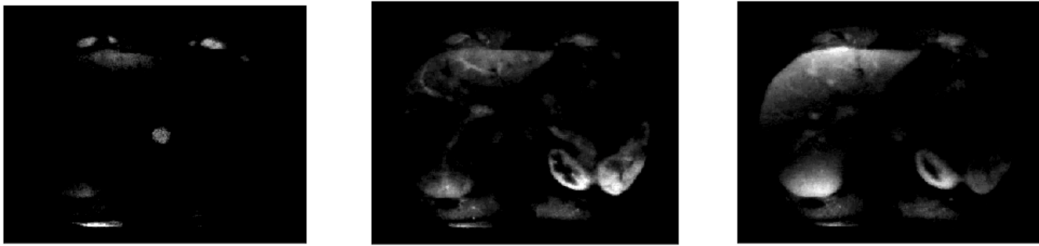


Figure 8: Comparing the  $l_1$ -ball, the horseshoe and the Bayesian lasso in different dimensionality and sparsity levels. The  $l_1$ -ball enjoys the smallest error and the closest estimation for  $c_0$ .

We use the posterior mean  $\hat{\theta}$  to compute the 2-norm error,  $\|\hat{\theta} - \theta^0\|_2$ . We also compute the estimated cardinality  $\hat{c}$  through averaging the number of non-zero entries of each posterior sample. Since the continuous shrinkage priors do not produce exact zero, we use an approximate measure of cardinality  $\hat{c} = \#\{\theta_i : |\theta_i| > \delta\}$  and we choose  $\delta = 0.1\sigma$  in this study.

As shown in Figure 8, Panel (a) and (b), the  $l_1$ -ball enjoys the smallest 2-norm in both cases. Between the two continuous priors, the horseshoe is more competitive especially when the model is sparse. Panel (c) and (d) shows that the  $l_1$ -ball gives a good estimation on the cardinality.

## Additional Comparison of the Sparse Change Detection



(a) The sparse change at  $t = 15$ . (b) The sparse change at  $t = 35$ . (c) The sparse change at  $t = 75$ .

Figure 9: The sparse change component  $S_t$  with a time-invariant background. Compared to Figure 6, these sparse estimates fail to reveal details under the slowly changing background: (a) does not highlight the aorta enhancement enough; (b) and (c) involve too much light changes, so that the detailed liver and portal vein enhancement are blurred.